Identification and characterization of bladder cancer by low-resolution fiber-optic Raman spectroscopy

Hao Chen[1, 2] | Xin Li[3,*] | Neil Broderick[4, 2] | Yuewen Liu[5] | Yajun Zhou[5] | Jianda Han[6, 7] | Weiliang Xu[1, 2, *]

[1]Department of Mechanical Engineering, the University of Auckland, Auckland 1010, New Zealand

[2]The Dodd-Walls Centre for Photonic and Quantum Technologies, PO Box 56, Dunedin 9054, New Zealand

[3]Department of Urology, the General Hospital of Shenyang Military, Shenyang 110000, China

[4]Department of Physics, the University of Auckland, Auckland 1010, New Zealand

[5]Jinzhou Medical University, Jinzhou, China

[6]College of Computer and Control Engineering, Nankai University, China

[7]State Key Lab of Robotics, Shenyang Institute of Automation, Chinese Academy of Sciences, China

*** Correspondence**

Xin Li, Department of Urology, the General Hospital of Shenyang Military, Shenyang 110000, China

Email: 18909882229@qq.com

Weiliang Xu, Department of Mechanical Engineering, the University of Auckland, Auckland 1010, New Zealand

Email: p.xu@auckland.ac.nz

Raman spectroscopy has been proved to be a promising diagnostic technique for various cancers detection. A major drawback for its clinical translation is the intrinsic weakness of Raman effects. Highly sensitive equipment and optimal measurement conditions are generally applied to overcome this drawback. However, these equipment are usually bulky, expensive and may also be easily influenced by surrounding environment. In this preliminary work, a low-resolution fiber-optic Raman sensing system is applied to evaluate the diagnostic potential of Raman spectroscopy to identify different bladder pathologies *ex vivo*. A total number of 262 spectra taken from 32 bladder specimens are included in this study. These spectra are categorized into 3 groups by histopathological analysis, namely normal bladder tissues, low-grade bladder tumors and high-grade bladder tumors. Principal component analysis (PCA) fed artificial neural network (ANN) are used to train a classification model for the spectral data with 10-fold cross-validation and an overall prediction accuracy of 93.1% is obtained. The sensitivities and specificities for normal bladder tissues, low-grade bladder tumors and high-grade bladder tumors are 88.5% and 95.1%, 90.3% and 98%, and 97.5% and 96.4%, respectively. These results demonstrate the potential of using a low-resolution fiber-optic Raman system for *in vivo* bladder cancer diagnosis.

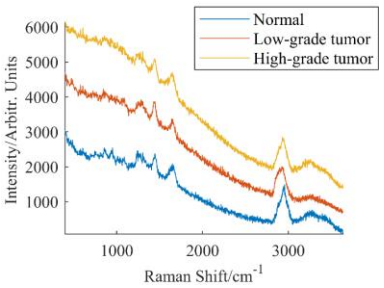

KEYWORDS
Raman spectroscopy, bladder cancer, PCA, ANN, low-resolution

1 | INTRODUCTION

Bladder cancer is the ninth most frequently-diagnosed cancer throughout the world and ranks as thirteenth in terms of mortality rates [1]. Besides, it also has the highest recurrence rate of any type of cancer with over 50% recur within 5 years of initial diagnosis, and a significant proportion has a tendency of progression [2, 3]. Therefore, early and thorough detection and complete resection of bladder cancer are essential for improving prognosis for patients. The majority of bladder cancers (about 90%) are transitional cell carcinomas (TCC), which grow in bladder mucosa, and most of them are non-muscle invasive.

The gold standard for bladder cancer diagnosis is cystoscopy followed by histopathological examinations of biopsies. This method is highly subjective, which means the decision is made depending on pathologists' experience. And it also has a certain extent of both intra- and inter-observer variability. Currently, transurethral resection of bladder tumors (TURBT) is the primary procedure for early bladder cancer diagnosis and treatment. Unfortunately, conventional

This article has been accepted for publication and undergone full peer review but has not been through the copyediting, typesetting, pagination and proofreading process, which may lead to differences between this version and the Version of Record. Please cite this article as doi: 10.1002/jbio.201800016

white light-guided cystoscopy (WLC) has a low sensitivity to small papillary tumors, carcinoma in situ (CIS), and even low grade tumors with different stages. Photodynamic diagnosis (PDD) significantly enhances the sensitivity from 75% to 95% (approximately) compared with WLC [4, 5]. However, it suffers from a high false positive rate which hinders its full implementation in clinical environment. Additionally, the need for long-term surveillance after TURBT makes bladder cancer to be one of the most expensive disease to manage [6]. Therefore, an economical and objective method that can provide high sensitivity and specificity to bladder cancer detection is strongly needed.

To meet the unmet clinical requirements of bladder cancer diagnosis, various methods including imaging techniques [7-10] and spectroscopic techniques [11-13] have been explored by groups over the last decades. Particularly, Raman spectroscopy has an outstanding performance and has been applied to cancer diagnosis in various organs [14-19]. It is capable of interrogating and characterizing chemical compositions of tissues at a molecular level with minimal disturbance. It is an inelastic scattering process of incident laser light, where a small portion of scattered photons experience shifts in frequency. Measuring the frequency-shifted photons results in a spectrum of Raman peaks, which provides fingerprint information of specific chemical bonds. Non-destructiveness and without a need of sample preparation make it very suitable for *in vivo* on-line bladder cancer diagnosis.

A critical disadvantage of Raman spectroscopy is that the Raman effect is so weak that only 1 in 10^6 to 10^8 photons undergoes Raman scattering, which makes it extremely difficult to obtain high quality spectra using low laser power and short integration time to meet the requirements of *in vivo* applications. Normally, this drawback is overcome by employing highly sensitive and accurate equipment and conducting measurements under optimal conditions. These equipment are usually bulky, expensive and difficult to maintain, which may contribute to additional cost to patients.

Schie et al. [20] proved that spectral resolution of Raman spectra have insignificant influence on the classification results of three cancer cell lines, which indicates that the instruments used for biological Raman applications can be considerably simplified and the cost can be significantly reduced. The long-term goal of our research is to realize the clinical implementation of *in vivo* online bladder cancer diagnosis using fiber-optic Raman technique. In this preliminary study, instead of using bulky and expensive instruments, the feasibility of utilizing a relatively low-resolution fiber-optic Raman system for bladder cancer identification is examined *ex vivo*. Combined with principal component analysis (PCA) and artificial neural network (ANN), this system is used to discriminate normal bladder tissue from low-grade and high-grade TCC of bladder. Importantly, comparable or even better performance in terms of specificity and sensitivity of classifying different pathological groups to those of previous studies using large and heavy instruments is obtained.

2 | MATERIALS AND METHODS

The data collection was conducted at the General Hospital of Shenyang Military with ethics approval to collect bladder tissue samples for Raman spectroscopy experimentation from the Ethics Committee of the same hospital. Fully informed consent was obtained from patients prior to sample collection. All the data processing algorithms were developed in Matlab 2017b (The Mathworks Inc., USA) with neural network toolbox.

2.1 | Sample collection and preparation

A total number of 32 bladder biopsy specimens from 10 patients were collected at cystoscopic procedures including TURBT. After resection from the patients, the samples were immediately placed in a 3ml cryovial and snap frozen in liquid nitrogen. Histological sections were cut from each sample and stained with haematoxylin and eosin (H&E) for standard histopathological analysis. The remaining samples were retained in liquid nitrogen until Raman spectroscopic measurements. All H&E-stained tissue sections were examined by an experienced histopathologist without information on patients' history and Raman spectroscopy. The samples were categorized into three groups according to their grades: normal bladder tissue, low grade bladder tumor and high grade bladder tumor. These three groups are commonly identified bladder pathologies by histopathological analysis in the General Hospital of Shenyang Military. **TABLE 1** shows a summary of sample number and spectra taken from each pathological group.

TABLE 1 The number of samples and spectra taken from each pathological group.

Pathological group	Number of samples	Number of spectra
Normal	11	78
Low-grade TCC	7	62
High-grade TCC	14	122
Total	32	262

2.2 | Raman spectroscopy procedures

The Raman spectra were measured *ex vivo* with a portable fiber-optic Raman system (Figure 1(a)). The system consists of four major parts: a 785 nm continuous laser source (FC-D-785, CNI Optoelectronics Technology Co., Ltd, Changchun, China), a handheld fiber-optic Raman probe (Emvision LLC, Florida, USA), a compact spectrometer (TG-Raman 785-1100 nm, CNI Optoelectronics Technology Co., Ltd, Changchun, China) coupled with a Hamamatsu S11510 CCD detector (Hamamatsu Photonics, Hamamatsu, Japan), and a computer. The laser source is able to provide up to 450 mW stable laser light after several minutes warmup. The probe is a 7-around-1 design with one laser delivery fiber surrounded by seven collection fibers. All fibers in the probe are 300-micron core low-OH, 0.22 NA fibers. At the distal end, a band-pass filter is placed in front of the excitation fiber and a ring-shaped long-pass filter is placed in front of the collection fibers. The probe with a 2.1 mm outer diameter illuminates a 0.5mm-

diameter area and samples up to a depth of ~ 1mm. In order to further eliminate the Rayleigh scattering light collected by the collection fiber, an additional long-pass filter (BLP01-785R-25, Semrock, IDEX Health & Science, LLC, New York, the USA) is added before the collected signal goes into the spectrometer. Instead of using a bulky spectrometer with high precision and resolution, a compact spectrometer which provides a spectral resolution of ca. 36 cm^{-1} was used. The CCD detector has a pixel size of 14 × 14 μm and has a quantum efficiency of 40% at 1000nm. Although the spectral resolution is not very high, it can provide the whole range spectrum (from 400 cm^{-1} to 3500 cm^{-1}) in one measurement without the need of moving gratings.

Before taking Raman measurements, samples were taken out from liquid nitrogen and passively thawed to room temperature (about 25 °C). This technique has been proved to be efficient to preserve the biochemistry of samples close to their original states in live tissue [21]. Samples were carefully placed on a small metal plate and orientated with the urothelium facing up to receive incident laser beam. This placement imitates *in vivo* measurement geometry. Samples were kept wet in normal saline during measurement. Spectra were taken by placing the probe head in slightly contact with samples. Figure 1(b) illustrates the measurement geometry. The collection time for each spectrum is 1s and the laser power at the sample is about 150mW. According to the size of each sample, two to five measurement points were randomly selected and two spectra were taken at each point. As a result, a total number of 262 spectra were obtained.

2.3 | System calibration and data pre-processing

The wavenumber response of the spectrometer was calibrated using an Oriel 6031 pencil style calibration lamp (Newport Corp., California, the USA). Six emission lines were carefully chosen to be resolvable by the spectrometer without any confusion to calculate the calibration coefficients. After calibration, all the spectra were grouped according to their histopathological analysis results and then preprocessed through the following procedure:

1) remove spikes caused by cosmic ray effect or instrument defects by performing linear interpolation at suspicious locations;
2) reduce random noise using wavelet denoising
3) perform standard normal variate (SNV) to transform the measured spectra to a similar scale
4) apply airPLS [22] to remove baseline
5) perform extended multiplicative signal correction (EMSC) [23]

2.4 | Multivariate analysis

The preprocessed data were then used to train a diagnostic classification model which is capable of identifying different pathologies. Principal component analysis (PCA) was first applied for data compression. PCA is an unsupervised multivariate analysis method that creates a new set of orthogonal principal components (PCs) to represent the original data matrix. The order of PCs indicates their explained proportion of variance. PC1 explains the biggest proportion of variance, PC2 explains the second biggest, etc. By selecting the first several PCs which can explain a most part of data variance (e.g. 90%), PCA is able to realize data compression. A two sample student t test was applied on the selected PCs to identify which one or several have the diagnostic significance for bladder cancer identification. Then the PCs with diagnostic significance were used to train a two-layer feedforward artificial neural network (ANN). ANN is a powerful self-adaptive and data-driven pattern recognition method with the ability of capturing nonlinear and complex underlying characteristics of data under investigation. Another reason for choosing ANN as the model training method in this study, rather than other widely used classification method such as linear discriminant analysis (LDA) and support vector machine (SVM), is that after dozens of trials ANN constantly outperformed LDA and SVM in terms of classification accuracy (results not given). Ten-fold cross-validation was used to evaluate the PCA-ANN model and the model training parameters are listed in TABLE 2. Unlike conventional 10-fold cross-validation which usually divides the original dataset into only a training set and a validation set, the cross-validation procedure in this study

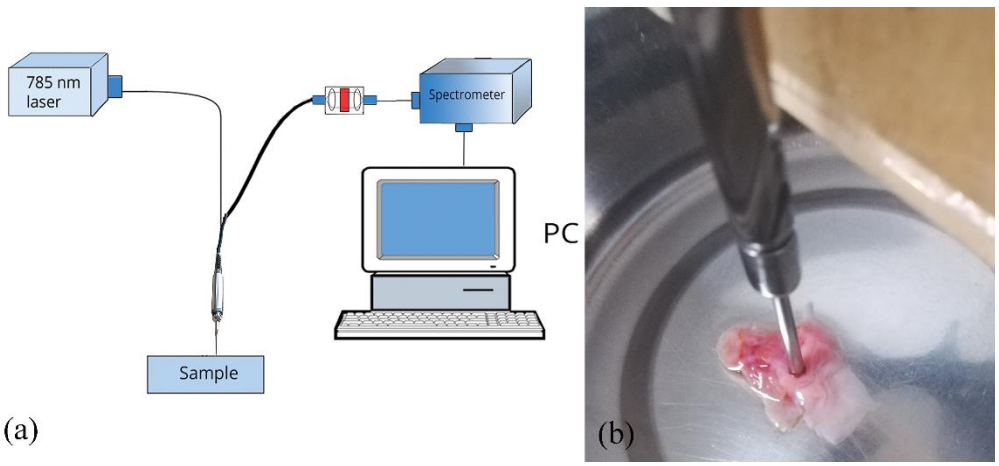

FIGURE 1 (a) The low-resolution fiber-optic Raman sensing system used in this study (an additional long-pass filter stage is added before the collected signal goes in to the spectrometer); (b) probe placement during measurement.

was done by dividing the original data set into a training set, a validation set and a test set. More specifically, the cross-validation procedure was performed through the following steps:

1) randomly divide the original spectral datasets into 10 subsets;
2) the first and second subsets were assigned as validation set and test set, respectively. And the remaining 8 subsets were assigned as training set;
3) train the ANN model;
4) increase the indices of validation set and test set by 1 and the remaining 8 subsets were assigned as training set;
5) repeat steps 4) and 3) until all subsets have been assigned as validation set and test set once;
6) select the model with the best performance as the final PCA-ANN model. The best performance is decided by the mean squared prediction error of validation set.

TABLE 2 Training parameters of ANN.

Parameters	Value
Number of hidden neurons	10
Training function	Scaled conjugate gradient
Performance function	Mean squared error(MSE)
Maximum iteration	100
Validation checks	6 more iterations after local minima
Cross-validation	10-fold cross-validation

3 | RESULTS AND DISCUSSION

The average spectra of each group after preprocessing are shown in **Figure 2(a)** and the offset mean spectra ± standard deviation of each group are provided in **Figure 2(b)**. To illustrate how strong the fluorescence background in the raw data is, example original spectra of the three groups are provided in **Figure S1** (Supplementary Information). Due to low spectral resolution of the spectral acquisition system, the number of recognized Raman peaks are very limited. Peaks close to each other are very likely to be overlapped and recognized as a bigger peak. For example, the wide peak in the range between 1500 cm^{-1} and 1700 cm^{-1} may be an overlap of 4 smaller peaks (1546, 1576 1608 and 1654 cm^{-1}) and the peak in the range of 1000 cm^{-1} to 1100 cm^{-1} might be a combination of 1052 cm^{-1} and 1077 cm^{-1} [24]. The mean spectra of the three classes exhibits very similar profile. However, significant differences in terms of peak locations and peak intensities can still be observed. The difference spectra between every two groups of the three are given in **Figure 3** where clear differences can be observed. Tentative assignments of major peaks shown in **Figure 2 and 3** are given as follows[25-30]: 481 cm^{-1}(glycogen), 621cm^{-1} (S-S disulfide stretch in proteins), 683 cm^{-1} (C-S twist, tyrosine), 755 cm^{-1} (Symmetric breathing of tryptophan), 830 - 853 cm^{-1} (tyrosine), 937 cm^{-1} (C-C stretching in protein), 1003 cm^{-1} (symmetric ring breathing of phenylalanine), 1077 cm^{-1} (C-C and C-O in lipids and glucose), 1220-1300 cm^{-1} (amide III, C-N stretching mode of proteins, collagen), 1315 cm^{-1} (CH_3CH_2 twisting mode of lipids and collagen), 1342 cm^{-1} (DNA/RNA and C-H deformation of proteins and tryptophan), 1445 cm^{-1} (CH_2 bending, collagen/phospholipids), 1585 cm^{-1} (phenylalanine), 1640 cm^{-1} (amide I, proteins), 2817 - 2875 cm^{-1} (CH_2/CH_3 symmetric stretching of lipids), and 2929 – 2940 cm^{-1} (CH_2 asymmetric stretch).

In Figure 2(a), some bands show clear progressive trend, either increasing or decreasing, from normal bladder tissue to high-grade bladder tumor. For example, the bands at 621 cm^{-1}, 755 cm^{-1}, and 1220-1300 cm^{-1}. Some bands at 481 cm^{-1}, 1077 cm^{-1}, 1445 cm^{-1}, and 1640 cm^{-1}, do not show a clear trend. Some reasons can be used to explain this phenomenon. Firstly, the high-volume probe has a sampling depth up to ~1mm. A considerable proportion of Raman signal may be derived from the submucosa and muscle layer. The collected Raman spectra in some way reflect the invasiveness of cancerous cells which is not taken into account in this study. Further study to find the influence of invasive stages of bladder cancer on the collected spectra using the same low-resolution system still needs to be done in the future. This can be done by classifying the samples according to both their stages and grades information. Secondly, the parameters used in the pre-processing step have a great impact on the resulting mean spectra. For example, a parameter λ that controls the penalty item in airPLS needs to be tuned by the user (set as 10^8 in this

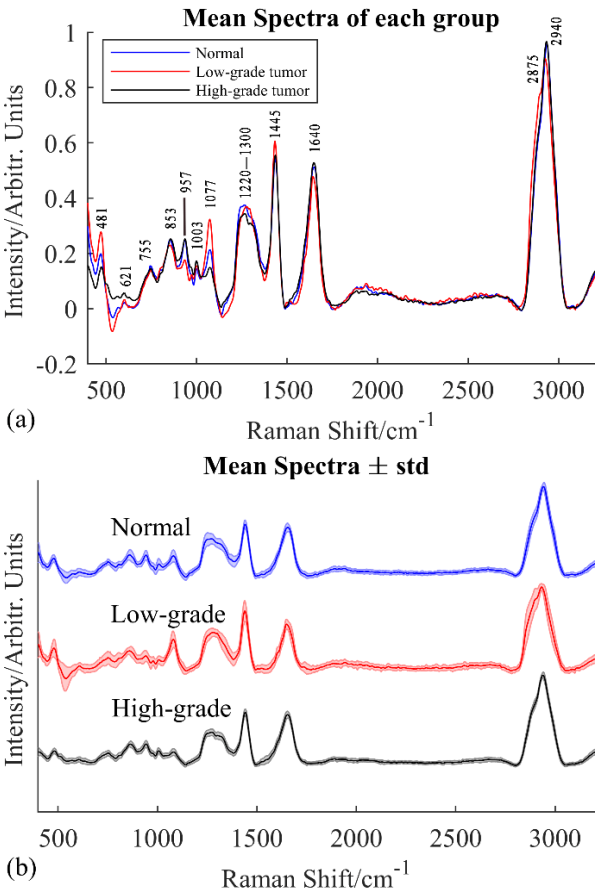

FIGURE 2 Comparison of bladder tissue classes: (a) mean spectra of each class; (b) mean ± standard deviation of each class (offset)

study). Adjusting this parameter may lead to a huge difference on the mean spectra.

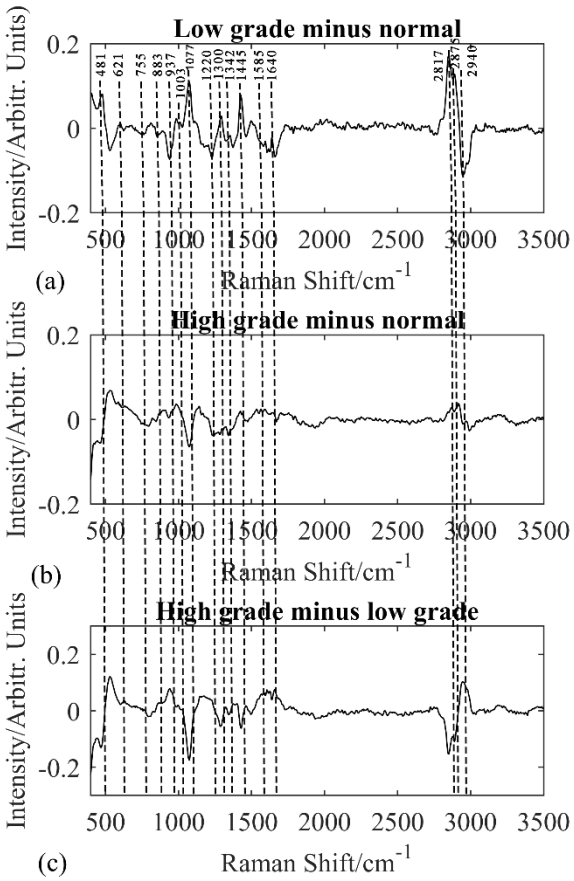

FIGURE 3 Difference spectra between every two pathological groups: (a) low grade tumor minus normal bladder tissue, (b) high grade tumor minus normal bladder tissue and (c) high grade tumor minus low grade tumor.

PCA was then applied on the preprocessed spectral data for dimensionality reduction. After calculation, the first 43 PCs can explain over 90% of total variance in the data matrix and were selected for further analysis. A PCA score plot of normal, low-grade tumor and high-grade tumor along PC1, PC2 and PC3 is presented in Figure 4. Each colored point in the scatter plot represents a single spectrum. PC1 explained the most part (about 33%) of total variance of the spectral data, while PC2 and PC3 explained about 18% and 8%, respectively. As seen in Figure 4, spectra groups into three classes with little confusion according to corresponding pathologies as expected. More precisely, most spectra of normal bladder tissue (blue crosses) fall into the range where PC1 ∈ [-1, 1], PC2 ∈ [-0.5, 1] and PC3 ∈ [-0.5, 0.5]; spectra of low grade tumor tissues (red circles) all have positive PC2 values; most spectra of high-grade tumor tissues (pink triangles) fall into the range where PC1 ∈ [-1, 1], PC2 ∈ [-1. 0], and PC3 ∈ [-0.5, 1]. The spectra of low grade bladder tumor have a more dispersed distribution and may have some confusions with the other two groups. This can be explained by the characteristics of low-grade bladder tumors. Low-grade tumors look more like normal bladder tissues than high-grade tumors. In addition, grade 1 tumors are low-grade tumors and grade 3 tumors are high-grade tumors whereas Grade 2 tumors can be categorized into either low grade or high grade.

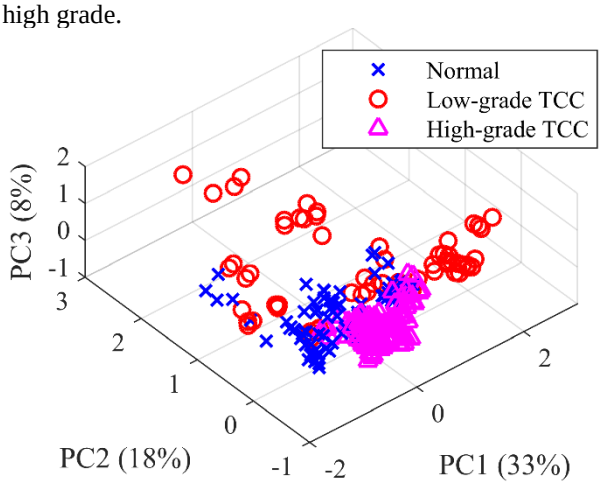

FIGURE 4 Score plot of normal, low-grade and high-grade tumor tissue along the first three PCs. The numbers in parentheses indicate the explained variance by the corresponding PC.

A two-sample student t test was performed on the selected PC scores to extract the ones with significance in distinguishing different bladder pathologies ($p<0.05$). **Figure 5** shows the t test results (1-p value) along the first 43 PCs. Only the first and second PCs show the ability to identify every bladder pathology. Other PCs either have no difference in identify each pathology or can only distinguish two of the three groups. In order to preserve the most useful information, PCs with significance in differentiating any two groups were found and examined. PCs with indices of 1, 2, 3, 4, 5, 6, 9, 12, 14, 16, 21, 24, 32, and 35 were selected and their corresponding PC loadings are provided in **Figure S2**. Clear spectral vibrations can be found in the first six PC loadings. Noise is the major component in the remaining selected PC loadings. As a result, the first six PCs were assigned as significant PCs and fed into an ANN training model.

The supervised ANN model applied in this study is a two-layer feedforward neural network with backpropagation training. After several trials with different number of hidden neurons set in the first layer, the model performance in terms of overall accuracy did not change significantly. So, the number 10 was employed. The structure of the network is illustrated in **Figure 6** where W represents applied weights and b represents bias vector. The inputs of the network are the 14 significant PCs and the outputs are the pathological predictions of each spectrum. The training targets are the histopathological analysis results of each bladder tissue samples.

Ten-fold cross-validation was performed to evaluate the performance of the PCA-ANN models and select the one with the best performance as the final model. Mean squared error (MSE) of validation set was chosen as the performance evaluation criterion for each model. The model with the lowest MSE was selected as the final model. Six more iterations in the model training process were performed after a local minimum was reached. If no better results were found, the local minimum would be considered as the best

performance for the model and the iteration procedure stopped. The final model's performance is presented in **Figure 7**. The point of intersection of the two dashed lines indicates the best validation set performance which is found at iteration 13. Before the best validation performance is reached, the MSE values of the three sets show similar gradually decreasing trend and no significant increase is observed in the performance of test set (red line). This behavior indicates that there is no or little over-fitting in the final model.

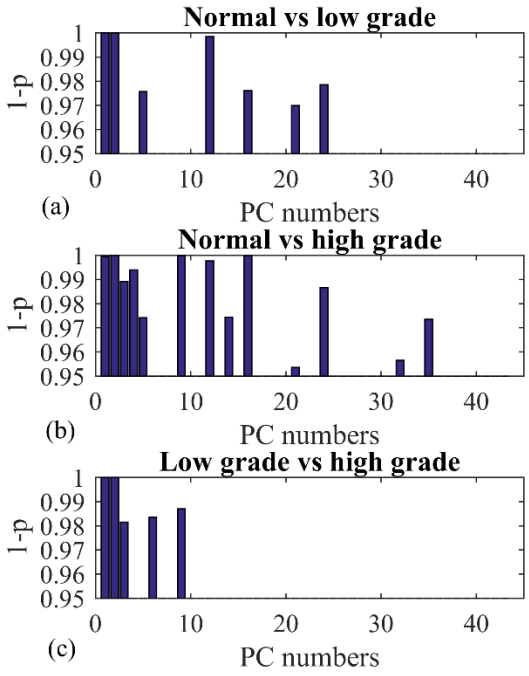

FIGURE 5 Two-sample student t test results between groups (value 1-p)

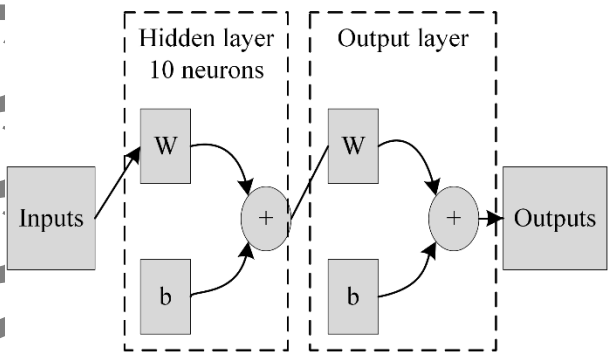

FIGURE 6 The architecture of the two-layer feedforward ANN with W and b represents weight vector bias vector applied.

The confusion matrices of training set, validation set, test set and overall data are listed in **TABLE 3**. The confusion matrix of training set shows that there are 15 misclassifications of 210 spectra, which gives a 92.9% classification accuracy. For the validation set, only 1 spectrum of normal tissue was wrongly categorized into high-grade tumor and other spectra within this set were all correctly classified (96.2% classification accuracy). Two misclassifications were found in the test set leading to an accuracy of 92.3%. The overall classification accuracy is 93.1%. Those misclassifications may be attributed to spectroscopy-histopathology mismatches. For example, a spectrum might be taken at a normal bladder site on the sample which was labeled as high-grade tumor tissue by pathological analysis.

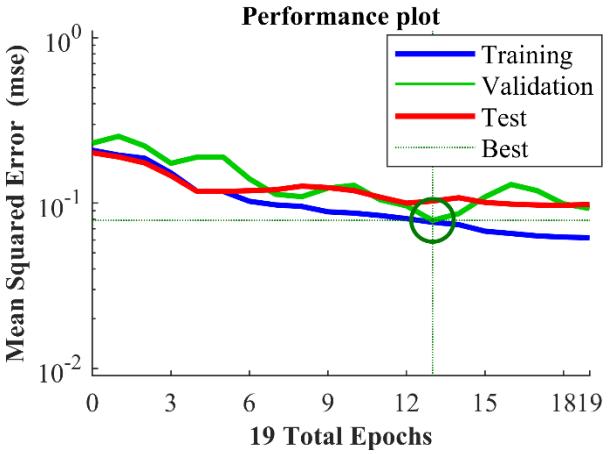

FIGURE 7 Performance of the final ANN model

TABLE 3 Confusion matrices of training set, validation set, test set and overall data, where Normal represents normal bladder tissue, Low represents low-grade tumor, and High represents high-grade tumor

ANN model predictions		Pathology analysis		
		Normal	Low	High
Training set	Normal	52	4	3
	Low	4	45	0
	High	4	0	98
Validation set	Normal	11	0	0
	Low	0	5	0
	High	1	0	9
Test set	Normal	6	2	0
	Low	0	6	0
	High	0	0	12
Overall	Normal	69	6	3
	Low	4	56	0
	High	5	0	119

These classification results that were translated to sensitivity and specificity for each bladder tissue group are shown in **TABLE 4**. The sensitivities and specificities are all over 88.5% for all the three groups which indicates that the PCA-ANN classification model has a good performance in recognition of these three types of bladder tissues. To be more exact, the sensitivity and specificity for normal bladder tissues are 88.5% and 95.1%, respectively. For low bladder tumor tissues, it has a sensitivity of 90.3% and a specificity of 98%. The sensitivity for high-grade tumor tissues is the highest (97.5%) as expected. This can be explained by the

distinct features of high-grade tumors. Unlike low-grade bladder tumors that are usually well differentiated, a high grade tumor looks very abnormal in appearance and is poorly differentiated.

To further elucidate the performance of the low-resolution fiber-optic Raman system combined with the PCA-ANN model, the receiver operating characteristics (ROC) curves for each pathological group are also examined (**Figure 8**). The solid grey line represents a random model with 50% accuracy. For a perfect prediction model, the 'elbow point' of each curve should be at the top left corner and the area under curve (AUC) should be 1. As can be easily recognized, the ROC curves for the three groups are very close to perfect classification. The AUCs are 0.9695 for normal bladder tissue (blue line), 0.9868 for low-grade bladder tumor (green line) and 0.9931 for high-grade bladder tumor (red line).

Although the spectral resolution of the fiber-optic Raman sensing system in this study may not be comparable with that of studies done by other research groups, the results above have demonstrated the effectiveness of the low-resolution system together with PCA-ANN classification in identifying normal bladder tissues, low-grade bladder tumors and high-grade bladder tumors.

TABLE 4 Sensitivity and specificity for each pathological group.

Pathological group	Sensitivity	Specificity
Normal	88.5%	95.1%
Low-grade TCC	90.3%	98%
High-grade TCC	97.5%	96.4%
Overall accuracy	93.1%	

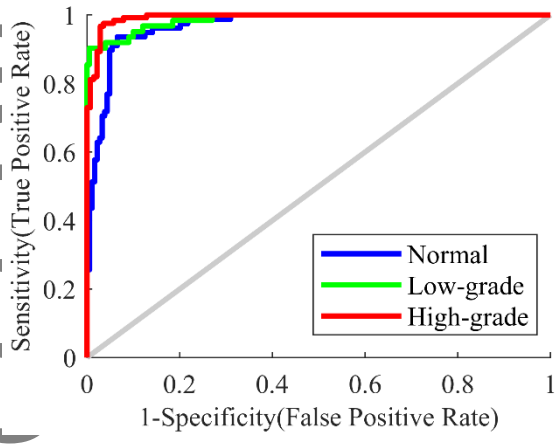

FIGURE 8 Receiver operating characteristic (ROC) curves of the PCA-ANN model for each pathological group. The blue line stands for normal bladder tissue and the AUC is 0.9695; the green line stands for low-grade bladder tumor and the AUC is 0.9868; the red line stands for high-grade bladder tumor and the AUC is 0.9931; the solid grey line stands for a 50%-accuracy random model.

4 | CONCLUSION

In conclusion, this preliminary study demonstrates the potential of using a relatively low-resolution fiber-optic Raman sensing system for bladder cancer diagnosis. A total number of 32 bladder tissue samples including normal bladder tissues, low-grade bladder tumors and high-grade bladder tumors were included in this study. With the help of a specially trained and cross-validated PCA-ANN classification model, an overall diagnostic accuracy of 93.1% for the three types of bladder tissue was obtained. The sensitivities and specificities for normal bladder tissues, low-grade bladder tumors and high-grade bladder tumors are 88.5% and 95.1%, 90.3% and 98%, and 97.5% and 96.4%, respectively. A disadvantage of this study is the limited number and diversity of samples. A bigger and more comprehensive sample collection may have influence on the PCA-ANN model's performance. Although this study proved the potential of applying low-resolution Raman system for bladder cancer diagnosis, further research works are still strongly needed to translate this technique to clinical applications.

CONFILICT OF INTEREST

The authors declare no conflict of interest.

AUTHOR BIOGRAPHIES

Please see Supporting Information online.

REFERENCES

[1] S. Antoni, J. Ferlay, I. Soerjomataram, A. Znaor, A. Jemal and F. Bray, Eur. Urol. **71**, 96-108 (2017).

[2] L. T. Kerr, T. M. Lynn, I. M. Cullen, P. J. Daly, N. Shah, S. O'Dea, A. Malkin and B. M. Hennelly, Anal. Methods. **8**, 4991-5000 (2016).

[3] S. Li, L. Li, Q. Zeng, Y. Zhang, Z. Guo, Z. Liu, M. Jin, C. Su, L. Lin and J. Xu, Sci. Rep. **5**, 9582 (2015).

[4] S. Denzinger, M. Burger, B. Walter, R. Knuechel, W. Roessler, W. F. Wieland and T. Filbeck, Urology **69**, 675-679 (2007).

[5] D. I. Daniltchenko, C. R. Riedl, M. D. Sachs, F. Koenig, K. L. Daha, H. Pflueger, S. A. Loening and D. Schnorr, J. Urol. **174**, 2129-2133 (2005).

[6] Y. Lotan, A. M. Kamat, M. P. Porter, V. L. Robinson, N. Shore, M. Jewett, P. F. Schelhammer, D. Quale and C. T. Lee, Cancer **115**, 4096-4103 (2009).

[7] F. D. Birkhäuser, U. E. Studer, J. M. Froehlich, M. Triantafyllou, L. J. Bains, G. Petralia, P. Vermathen, A. Fleischmann and H. C. Thoeny, Eur. Urol. **64**, 953-960 (2013).

[8] E. C. Cauberg, D. M. de Bruin, D. J. Faber, T. M. de Reijke, M. Visser, de La Rosette, Jean JMCH and T. G. van Leeuwen, J. Biomed. Opt. **15**, 066013-066013-6 (2010).

[9] R. Wessels, D. De Bruin, D. Faber, T. Van Leeuwen, M. Van Beurden and T. Ruers, Lasers. Med. Sci. **29**, 1297-1305 (2014).

[10] E. C. Cauberg, S. Kloen, M. Visser, de la Rosette, Jean JMCH, M. Babjuk, V. Soukup, M. Pesl, J. Duskova and T. M. de Reijke, Urology **76**, 658-663 (2010).

[11] J. Ollesch, M. Heinze, H. M. Heise, T. Behrens, T. Brüning and K. Gerwert, J. Biophotonics. **7**, 210-221 (2014).

[12] P. Crow, A. Molckovsky, N. Stone, J. Uff, B. Wilson and L. WongKeeSong, Urology **65**, 1126-1130 (2005).

[13] B. W. De Jong, T. C. Bakker Schut, K. Maquelin, T. Van Der Kwast, C. H. Bangma, D. Kok and G. J. Puppels, Anal. Chem. **78**, 7761-7769 (2006).

[14] N. Bergner, T. Bocklitz, B. F. Romeike, R. Reichart, R. Kalff, C. Krafft and J. Popp, Chemometrics Intellig. Lab. Syst. **117**, 224-232 (2012).
[15] J. H. Demers, S. C. Davis, B. W. Pogue and M. D. Morris, Biomed. Opt. Express. **3**, 2299-2305 (2012).
[16] B. Brozek-Pluska, J. Musial, R. Kordek, E. Bailo, T. Dieing and H. Abramczyk, Analyst **137**, 3773-3780 (2012).
[17] M. A. Short, S. Lam, A. McWilliams, J. Zhao, H. Lui and H. Zeng, Opt. Lett. **33**, 711-713 (2008).
[18] J. Zhao, H. Lui, D. I. McLean and H. Zeng, Skin. Res. Technol. **14**, 484-492 (2008).
[19] I. Barman, N. C. Dingari, G. P. Singh, R. Kumar, S. Lang and G. Nabi, Anal. Bioanal. Chem. **404**, 3091-3099 (2012).
[20] I. W. Schie, C. Krafft and J. Popp, J. Biophotonics. **9**, 994-1000(2016).
[21] N. Stone, M. C. H. Prieto, P. Crow, J. Uff and A. W. Ritchie, Anal. Bioanal. Chem. **387**, 1657-1668 (2007).
[22] Z. Zhang, S. Chen and Y. Liang, Analyst **135**, 1138-1146 (2010).
[23] N. K. Afseth and A. Kohler, Chemometrics Intellig. Lab. Syst. 117, 92-99 (2012).
[24] W. Zha, Y. Cheng, W. Yu, X. Zhang, A. Shen and J. Hu, **12**, 045701 (2015).
[25]T. J. Harvey, E. C. Faria, A. Henderson, E. Gazi, A. D. Ward, N. W. Clarke, M. D. Brown, R. D. Snook and P. Gardner, J. Biomed. Opt. **13**, 064004-064004-12 (2008).
[26] R. E. Kast, G. K. Serhatkulu, A. Cao, A. K. Pandya, H. Dai, J. S. Thakur, V. M. Naik, R. Naik, M. D. Klein and G. W. Auner, Biopolymers **89**, 235-241 (2008).
[27] Z. Huang, A. McWilliams, H. Lui, D. I. McLean, S. Lam and H. Zeng, Int. J. Cancer. **107**, 1047-1052 (2003).
[28] M. S. Bergholt, W. Zheng, K. Lin, K. Y. Ho, M. Teh, K. G. Yeoh, J. B. Yan So and Z. Huang, **128**, 2673-2680 (2011).
[29] S. Li, Y. Zhang, Q. Zeng, L. Li, Z. Guo, Z. Liu, H. Xiong and S. Liu, **11**, 065603 (2014).
[30] A. C. S. Talari, Z. Movasaghi, S. Rehman and I. U. Rehman, **50**, 46-111 (2015).
[31] N. Stone, C. Kendall, N. Shepherd, P. Crow and H. Barr, J. Raman Spectrosc. **33**, 564-573 (2002).

SUPPORTING INFORMATION

Additional Supporting Information may be found online in the supporting information tab for this article.

Figure S1 Example original spectra of the three group.
Figure S2 Loadings of PCs with diagnostic significance.